Energy Storage Materials 18 (2019) 59–67

Contents lists available at ScienceDirect

Energy Storage Materials

journal homepage: www.elsevier.com/locate/ensm

Anion-immobilized polymer electrolyte achieved by cationic metal-organic framework filler for dendrite-free solid-state batteries

Hanyu Huo[a,b,1], Bin Wu[c,1], Tao Zhang[a], Xusheng Zheng[d], Liang Ge[c,*], Tongwen Xu[c,*], Xiangxin Guo[e,*], Xueliang Sun[f]

[a] State Key Laboratory of High Performance Ceramics and Superfine Microstructure, Shanghai Institute of Ceramics, Chinese Academy of Sciences, Shanghai 200050, China
[b] University of Chinese Academy of Sciences, Beijing 100049, China
[c] CAS Key Laboratory of Soft Matter Chemistry, iCHEM (Collaborative Innovation Center of Chemistry for Energy Materials), Department of Chemistry, School of Chemistry and Materials Science, University of Science and Technology of China, Hefei 230026, China
[d] National Synchrotron Radiation Laboratory, University of Science and Technology of China, Hefei, 230026, China
[e] College of Physics, Qingdao University, Qingdao 266071, China
[f] Department of Mechanical and Materials Engineering, University of Western Ontario London, Ontario, Canada N6A 5B9

ARTICLE INFO

Keywords:
Cationic metal-organic frameworks
Anion immobilization
High electrochemical performances
Dendrite-free solid-state batteries

ABSTRACT

The practical application of solid-state batteries (SSBs) is restricted by the growth of lithium dendrites, which could be attributed to uneven Li deposition mainly caused by the barrier of free anions in solid polymer electrolytes (SPEs). Herein, a novel cationic metal-organic framework (CMOF) is proposed to immobilize anions and guide Li^+ uniform distribution for constructing dendrite-free SSBs. The CMOF grafted with $-NH_2$ group protects the ether oxygen of polymer chains by hydrogen bonds, which extends the electrochemical window to 4.97 V. Such CMOF tethers anions by electrostatic interaction of charge carriers and the specific surface area as high as 1082 $m^2 g^{-1}$ further strengthens the effect of anion absorption on the surface of CMOF, leading to a high Li^+ transference number of 0.72. With the anion-immobilized composite electrolyte, the Li symmetrical cells can continuously operate for 400 h at 0.1 mA cm^{-2} and 200 h at 0.5 mA cm^{-2} without discernable dendrites, respectively. In addition, the SSBs constructed with $LiFePO_4$ and $LiFe_{0.15}Mn_{0.85}PO_4$ cathodes demonstrate excellent rate and cycle performances at 60 °C. These results indicate that anion immobilization by CMOF is a promising strategy to realize dendrite-free SSBs with high energy density and safety.

1. Introduction

With the growing demand of smart electronics and electric vehicles, developing new rechargeable batteries with high energy density is urgent [1]. Now, solid-state batteries (SSBs) received increasing attention due to their high energy density and high safety in comparison to commercial liquid cells. The use of solid-state electrolytes (SSEs) enables to construct batteries with high-voltage cathodes and Li metal anodes, thereby achieving high energy density for SSBs. In addition, the safety issues are well addressed by eliminating usage of flammable liquid electrolytes.

Among the potential SSEs, solid polymer electrolytes (SPEs) have been widely investigated based on poly(ethylene oxide) (PEO) polymer complex with alkali metal salts [2]. Various approaches have been employed to enhance the conductivity of SPEs, including polymer bending [3], grafting short oligomers onto polymer backbones [4], adding plasticizers or ionic liquid [5], and doping inorganic fillers [6,7]. Although much progress has been achieved, the hazardous Li dendrites penetrating through SPEs still greatly hinders the real application of SSBs [8,9,10]. The formation of dendrites leads to low coulombic efficiency, poor cycle performance, and short circuiting of SSBs at large [11,12]. To suppress dendrites, Monroe and Newman suggested the SSEs with shear modulus more than twice that of metallic Li, around 3.4 GPa as mechanical barriers, are pre-request [13]. However, such high moduli of SPEs is difficult to achieve without sacrificing ionic conductivity. And the intimate interfacial contact between SPEs and Li anodes is worsened due to the poor flexibility of high modulus of SPEs [14]. Archer and co-workers found that SPEs with moderate mechanical moduli can theoretically realize stable electrodeposition when a fraction anions are immobilized [15]. The results are consistent

* Corresponding authors.
E-mail addresses: geliang@ustc.edu.cn (L. Ge), twxu@ustc.edu.cn (T. Xu), xxguo@qdu.edu.cn (X. Guo).
[1] The author contributes equal to this work.

https://doi.org/10.1016/j.ensm.2019.01.007
Received 30 September 2018; Received in revised form 27 December 2018; Accepted 8 January 2019
Available online 09 January 2019

with the model of Sand's time, where the capability of anion immobilization can be quantified by Li^+ transference number (t_+) [16]. However, it is complicated to design anion trapping polymers with high t_+ by covalent bonding of anions to polymer chains [17]. And further modification of polymers is required considering the low conductivities. Surface-functionalized metal oxide particles as fillers were also doped in polymer electrolytes to tether anions by Lewis acid-base interaction, such as superacid ZrO_2, and acidic Al_2O_3 [18,19]. The acidic groups on ceramic particles share electron pairs with anions of Lewis base, thus realizing anion immobilization.

Recently, metal-organic frameworks (MOFs) as fillers in SPEs have emerged with improved ionic conductivities and superior interfacial properties. Yuan et al. proposed a novel MOF-5 in PEO polymers, which furnished highly conductive pathway along the interfaces for ion transportation [20]. The porous MOF-5 with large surface-to-volume is helpful for stabilizing interfaces between the electrolyte and Li metal. In addition, the SPEs with lightweight MOF as fillers are expected to render higher energy density of SSBs in comparison with those with heavyweight ceramic particles. Due to the tailor-making capability, the MOFs grafted with intended functional groups show the possibility for tethering anions in SPEs. As a class of micro-porous particles with high specific surface area, MOFs can further strengthen the effect of anion absorption and firmly trap anions around the surface, leading to a higher t_+ than ceramic particles.

Herein, we synthesized a novel cationic MOF (CMOF) by the nucleophilic substitution of grafted pyridine N based on UiO-66 (Zr-BDC MOF). The CMOF with specific surface area as high as 1082 $m^2 g^{-1}$ immobilizes anions via electrostatic interaction of charge carriers, which shows more effective than covalent bonding of polymers and Lewis acid-base interaction of metal oxides. Such anion-immobilized CMOF was dispersed in PEO/lithium bis(trifluoromethylsulphonyl) imide (LiTFSI) matrix to fabricate P@CMOF composite electrolytes by hot pressing method, rendering an order of magnitude higher conductivity than pure PEO electrolytes. The CMOF grafted -NH_2 group protects ether oxygen of PEO chains by hydrogen bonds as well as removes the impurities at interfaces, extending the electrochemical window to 4.97 V. The synergetic effect of CMOF with polymer results in anion trapping ability and dendrite-free Li anodes during Li deposition (Scheme 1). A small concentration gradient of Li^+ were obtained in the composite electrolyte according to simulation of finite element method, which prevents the formation of a large electrical field. Such anion-immobilized electrolytes used in Li metal cells with $LiFePO_4$ and $LiFe_{0.15}Mn_{0.85}PO_4$ cathodes exhibit excellent rate and cycle performances. It also shows the feasibility to use in flexible SSBs with high energy density.

2. Experimental section

2.1. Synthesis of D-UiO-66-NH_2

2-Aminoterephthalic acid (H_2ATA) (99%) and 2, 5-pyridinedicarboxylic acid were acquired from Alfa Aesar. The other reagents, including N, N-thdimethyl formamide (DMF), Trichloromethane($CHCl_3$), Zirconium(IV) chloride ($ZrCl_4$), Iodomethane (CH_3I) were all of analytical grade and commercially obtained from domestic chemical reagents companies.

H_2ATA (0.1413 g, 0.782 mmol), 2, 5-pyridinedicarboxylic acid (0.0430 g, 0.257 mmol) and $ZrCl_4$ (0.2396 g, 1.026 mmol) were added into a solution containing anhydrous DMF (30 mL), where acetic acid (0.663 g, 110 mmol) was used as the mineralizer. Then, the above solution was stirred at room temperature for 10 min and transferred into a 50 mL Teflon liner, followed by heating process at 120 °C for 24 h. After reaction, the resultant suspension was centrifuged in 10000 rpm for 10 minutes, repeatedly washed with DMF filtered, and dried under vacuum to obtain the bright-yellow solid product.

2.2. Synthesis of cationic D-UiO-66-NH_2 (CMOF)

Before synthesis, the D-UiO-66-NH_2 was activated by guest exchange and removal with DMF and $CHCl_3$. The crystals were then soaked in DMF and $CHCl_3$ for three days with fresh $CHCl_3$ added every 24 h at 80 °C, respectively. After 3 days of soaking, the crystals were stored in the last $CHCl_3$ solution until needed. The activated D-UiO-66-NH_2 was dipped in CH_3I/DMF(1:10) mixture solution for 5 days. At last, it was heated under vacuum at 358 K, washed with DMF and dried under vacuum to obtain the cationic D-UiO-66-NH_2 (CMOF).

2.3. Synthesis of P@CMOF membranes

PEO (Mv = 6 × 10^5 g mol^{-1}, Sigma-Aldrich) was dried at 60 °C overnight under vacuum before use. The LiTFSI (Sigma-Aldrich) was dried under vacuum at 100 °C for 10 h and stored in an Ar-filled glove box. The P@CMOF membranes were fabricated by hot pressing without any organic solvent. Predetermined volumes of CMOF powders, PEO, and LiTFSI were homogenously mixed and ground in a mortar to obtain a small rough ball. The EO to Li molar ratio was 10:1 and the content of CMOF powders varied from 0 to 22.5 vol%. Subsequently, the rough ball was sandwiched between two pieces of PTFE plates and transferred into a vacuum oven. By pressing for 2 h at 100 °C under 20 MPa, a uniform composite electrolyte membrane with the thickness of approximately 40 μm was successfully fabricated.

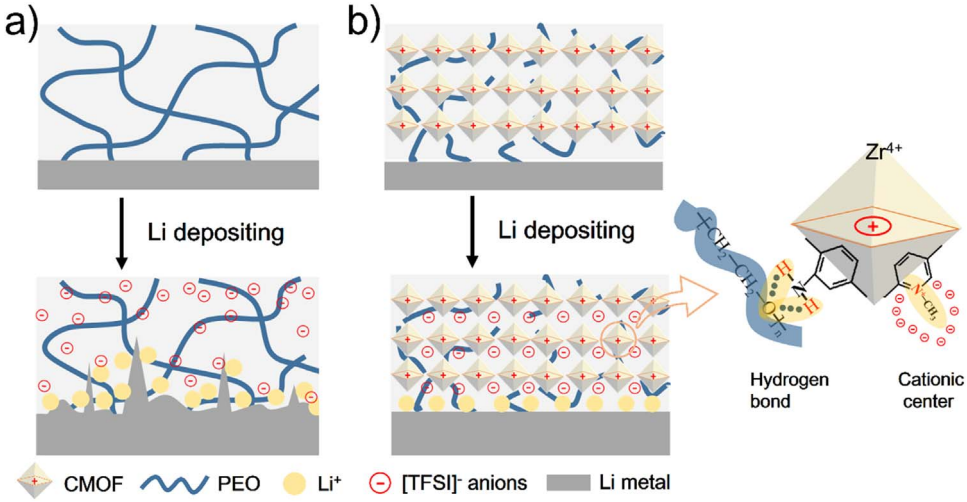

Scheme 1. Schematic of the Li deposition behavior with a) PEO(LiTFSI) electrolyte and anion-immobilized P@CMOF electrolyte.

2.4. Sample characterization

The crystalline structures of ingredients were examined by X-ray diffraction (XRD), using Cu K_α radiation (λ = 1.5406 Å) with 2θ in range of 5–60° and a step-width of 0.02°. The particle size distribution was tested by Zeta Plus (Brookhaven) laser particle size analyzer, using ethanol as solvent. The field emission scanning electron microscope (FESEM, Magellan 400) was employed to determine the morphologies of surface and cross-section of the samples. The cross-section of membranes was obtained by liquid nitrogen quenching and all the samples for FESEM were coated with a thin gold layer via sputter coating. N_2 adsorption/desorption isothermal was recorded on a Micromeritics ASAP 2020 HD88 tool. Thermogravimetric analysis (TGA) was tested from 30 to 500 °C at 10 °C min^{-1} under Ar atmosphere. Differential Scanning calorimeter (DSC) was carried out from 20 to 90 °C under Ar atmosphere. Raman spectra were obtained on a Bruker RFS100/S at the frequency range from 720 to 770 cm^{-1}. The Fourier transform infrared/attenuated total reflection (FT-IR/ATR) spectra were obtained using a Nicolet iS10 spectrometer. The ^{1}HNMR spectra were recorded on an AV III 400 NMR spectrometer (1H resonance at 400 MHz, Bruker), using D_2O-d6 (with tetramethylsilane as internal reference) as a solvent. The mechanical properties of electrolytes were tested by 5948 MicroTester Instron instrument. The X-ray photoelectron spectroscopy (XPS) characterization was determined by a Physical Electronics Escalab250 multi-technique system using monochromatic X-ray at a power of 350 W. Element analysis (EA) was investigated using an Elementar Vario EL III elemental analyzer (Elementar Analysensysteme GmbH (Germany)). The temperatures of combustion tube and reduction tube were set as 950 °C and 550 °C, respectively.

The N K-edge NEXAFS spectra were measured at the photoemission end-station at beamline BL10B in the National Synchrotron Radiation Laboratory (NSRL) in Hefei, China. A bending magnet is connected to the beamline, which is equipped with three gratings covering photon energies from 100 to 1000 eV. In this experiment, the samples were kept in the total electron yield mode under an ultrahigh vacuum at 5×10^{-10} mbar. The resolving power of the grating was typically E/△E = 1000, and the photon flux was 1×10^{-10} photons per second. Spectra were collected at energies from 390 to 410 eV in 0.2 eV energy steps.

2.5. Electrochemical measurement and cells assembly

The ionic conductivities of the P@CMOF were measured by the NOVOCONTROL spectrometer fitted with a temperature control system with the frequency range from 0.01 Hz to 40 MHz. The electrolytes were sandwiched between two stainless steels (SS), which were used as the block electrodes. The ionic conductivity σ was calculated based on the following equation:

$$= \frac{t}{RA} \quad (1)$$

Where t represents the thickness of the electrolyte membrane, R is the bulk resistance of electrolytes, and A refers to the contact area between electrolytes and electrodes.

The lithium ion transference number (t_+) was tested in a Li/SPE/Li cell (Autolab PGSTAT 302 N system). The symmetric battery was polarized with a DC voltage of 10 mV. The AC impedance spectroscopy before and after polarization were obtained. t_+ was calculated according to the following equation:

$$t_+ = \frac{I_{(t=\infty)}(\Delta V - I_{(t=0)R_{(t=0)}})}{I_{(t=0)}(\Delta V - I_{(t=\infty)R_{(t=\infty)}})} \quad (2)$$

Where ΔV is the applied DC polarization voltage (10 mV), $I_{(t=0)}$ and $R_{(t=0)}$ are the initial current and resistance value, respectively. $I_{(t=\infty)}$ and $R_{(t=\infty)}$ are the steady state current and resistance value after polarization for 3600 s, respectively.

The electrochemical window was examined by SS/electrolyte/Li cells, using linear sweep voltammetry (LSV), which was conducted from 2 to 6 V at a scan rate of 10 mV s^{-1} by Arbin BT-2000. Lithium dendrite growth was monitored by the Arbin BT-2000 using symmetric Li/electrolyte/Li coin cells with the current densities of 0.1 mA cm^{-2} and 0.5 mA cm^{-2} at 60 °C, respectively.

For cell performance test, the composite cathode slurry was coated on the electrolyte membranes, which consists of 50 wt% $LiFePO_4$, 30 wt% LiTFSI, 10 wt% PEO, 10 wt% Super-P. The specific density of active material is approximately 2 mg cm^{-2}. The $LiFePO_4$/electrolyte/Li 2025 coin-type cells with membranes of 19 mm diameter were charged and discharged between 2.8–3.8 V at varied current densities. The size of pouch cells were 60 × 80 mm^2 and the $LiFe_{0.15}Mn_{0.85}PO_4$ active material loading was about 120 mg in one cell.

2.6. Simulation of Li^+, anion, and electric potential distribution

Finite element method (FEM) conducted by COMSOL Multiphysics was employed to investigate the distribution of Li^+, anions, and electric potential in composite electrolyte. Two physical models of Electrostatic and Transport of Diluted Species were coupled to conduct FEM simulation. The plating/stripping of Li^+ was described by Butler-Volmer dynamical equation. The flux at the border of electrolyte was coupled with electrochemical reaction according to Faraday's Law. And the migration of Li^+ and anions driven by electric field were described by Nernst-Planck equation. All the parameters related to the electrolyte membranes were the practical measured values. The applied current density was 0.1 mA cm^{-2}.

3. Results and discussion

The synthesis process of CMOF was shown in Fig. 1**a**. The prototype MOF chosen here was UiO-66 based on $Zr_6O_4(OH)_4$ octahedron as inorganic building brick, which exhibits high surface area, linker independent, robust thermal and electrochemical stability [21]. The remarkable stability of UiO-66 in most solvents such as water, ethanol, acetone, dimethyl formamide (DMF), and benzene is the prerequisite for our functional modification. It could be attributed to the fact that each Zr octahedron is 12-fold connected to adjacent octahedral though 1, 4-benzene-dicarboxylate (BDC) linker [22]. Double ligands of 2-amino-terephthalic acid (H_2ATA) and 2, 5-pyridinedicarboxylic acid substituting BDC linker leads to the formation of intermediate MOF, D-UiO-66-NH_2. The -NH_2 group will facilitate the subsequent links with ether oxygen of PEO chains via hydrogen bonds to achieve a stable structure of composite electrolyte and extend the electrochemical window [23]. And the pyridine N with lone pair electrons as the nucleophilic reagent tends to substitute I of CH_3I and links with -CH_3 group [24–26]. After the nucleophilic substitution, the -N^+CH_3 charging center occurred and the CMOF was successfully synthesized. It should be noted that a small amount of free I^- from CH_3I released into the composite electrolytes was not harmful since LiI was used as additives into solid polymer electrolytes in previous studies [27]. As the X-ray diffraction (XRD) pattern shown in Fig. 1**b**, stimulated UiO-66 shows high crystallinity with two strong peaks at 7.36° and 8.48° corresponding to crystal face of (111) and (002), respectively [28]. The major diffraction peaks of D-UiO-66-NH_2 and CMOF are consistent with those for UiO-66, indicating the inherited crystal structure during fabrication process.

In order to verify that the double functional ligands retain in the structure of CMOF, both ^{1}HNMR spectrum and FT-IR were tested. Before testing ^{1}HNMR, the samples were dissolved in deuterium oxide solution of KOH and then centrifuged to remove all the precipitate. The ^{1}HNMR of supernatant liquid in Fig. 1**c** exhibits the signals of hydrogen resulting from the 2-aminoterephthalic acid, pyridine ring and methyl of UiO-66-NH_2, D-UiO-66-NH_2 and CMOF. Compared with the UiO-66-NH_2, the D-UiO-66-NH_2 and CMOF revealed the

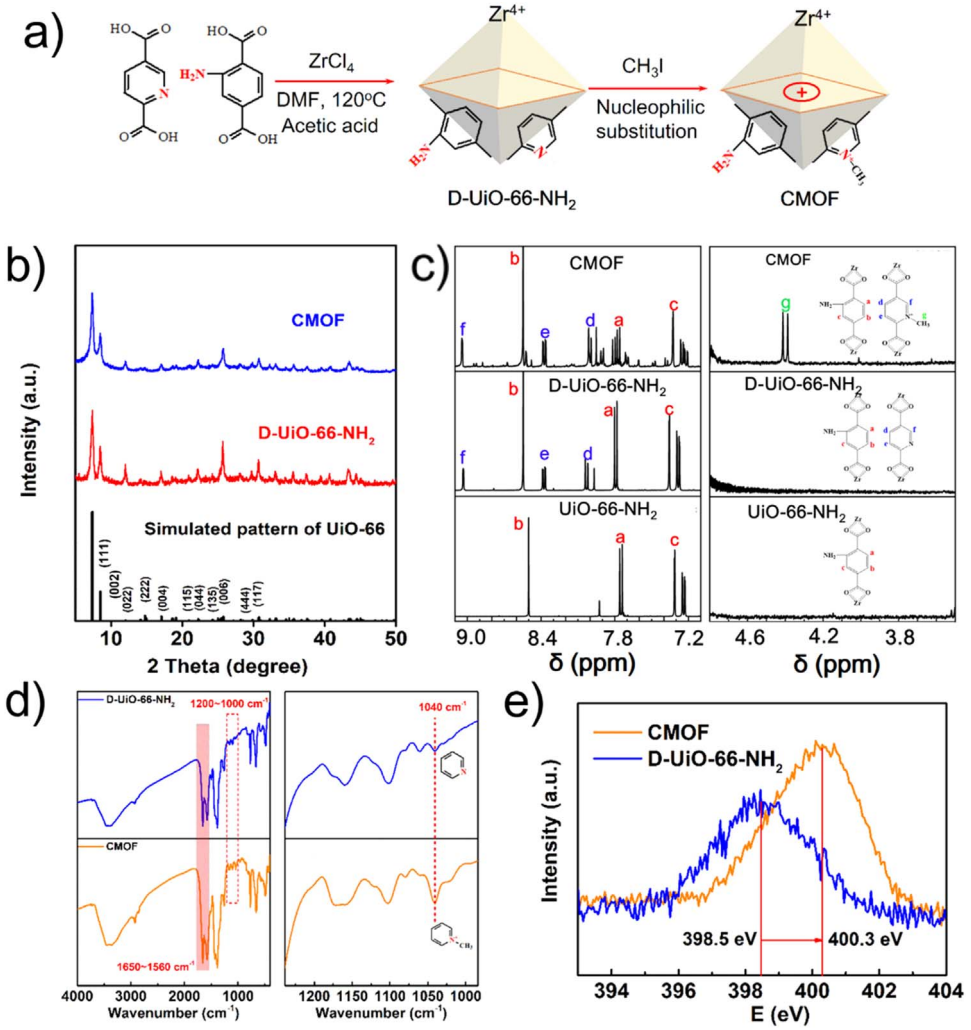

Fig. 1. a) Schematic illustration for the synthesis of CMOF. b) XRD patterns of simulated UiO-66, D-UiO-66-NH_2 and CMOF. c) ^{1}H NMR of UiO-66-NH_2, D-UiO-66-NH_2, and CMOF. d) FT-IR and e) NEXAFS spectra of D-UiO-66-NH_2 and CMOF.

peaks of two organic ligands, while the chemical shift of the methyl on pyridine N was also obtained to testify the charging properties of MOF. In the same time, the quaternization ratio of 15% for pyridine N was calculated according to the integral value of the peaks in Fig. S1 [29,30]. As the FT-IR shown in Fig. 1**d**, the peaks in the region of 1650–1560 cm^{-1} for aryl amines were obtained in D-UiO-66-NH_2 and CMOF, indicating the -NH_2 group remains active after charging process [31]. Additional peaks in the range of 1200–1000 cm^{-1} could be attributed to the pyridine ring, which is the significant ligand for charging process [32]. To confirm the cationic structure of as-obtained CMOF for anion immobilization, we performed a synchrotron near edge x-ray absorption fine structure spectroscopy (NEXAFS) to investigate the change in electron-photon energy of pyridine N before and after nucleophilic substitution. As shown in Fig. 1**e**, a significant shift on N K-edge peak from 846.5 eV to 848.3 eV was obtained, indicating the formation of covalent bond between pyridine N and -CH_3 [33]. Considering that the sulfur (S) is only in LiTFSI, the S contents of the D-UiO-66-NH_2 and CMOF were characterized after adsorption LiTFSI via Elemental Analysis (EA) and X-ray Photoelectron Spectroscopy (XPS), which can directly detect the anion-immobilizing process. As shown in Fig. S2, the increased S contents indicates that $TFSI^-$ was immobilized in the framework of CMOF by the electrostatic interaction. Although the uncharged D-UiO-66-NH_2 also has absorbability due to the high specific surface area, it shows poorer adsorption capacity than CMOF. The quaternary ammonium group of CMOF was clarified as the part to immobilize anions. The particle size of CMOF is approximately 100 nm, which tends to homogeneous dispersed in polymers compared with nano-sized ceramic particles (Fig. S3) [34]. Moreover, the specific surface area of CMOF is as high as 1082 $m^2 g^{-1}$ according to the N_2 adsorption/desorption isothermal tests, which is impossible for nano-sized ceramic fillers to achieve (Fig. S4). Such high specific surface area contributes to strengthen the effect of anion absorption by firmly trapping enough anions on the surface of CMOF, thus further improving t_+ [35]. Simultaneously, it generates superior interfaces between CMOF and PEO chains as highly conductive pathway for Li^+ migration beneficial from percolation effect [36].

The CMOF was incorporated into PEO polymer to fabricated P@CMOF composite electrolyte by hot pressing process, which is low-cost and environment-friendly. Compared with conventional solution-cast method, the toxic organic solvents were not used, which spontaneously reacts with lithium metal anode due to incomplete evaporation [37]. The as-obtained P@CMOF is translucent, freestanding, and bendable (Fig. 2a). The mechanical flexibility makes it feasible for fabricating flexible SSBs. The smooth and clear surface of P@CMOF in Fig. 2**b** can firmly adhere with electrodes, decreasing the interfacial resistance. In addition, the cross-section SEM in Fig. 2**c** shows a thickness of around 40 μm, where CMOF particles are well distributed in PEO polymer. The XRD pattern shows that the P@CMOF integrates the typical peaks of CMOF and PEO, especially the periodic fine structure of

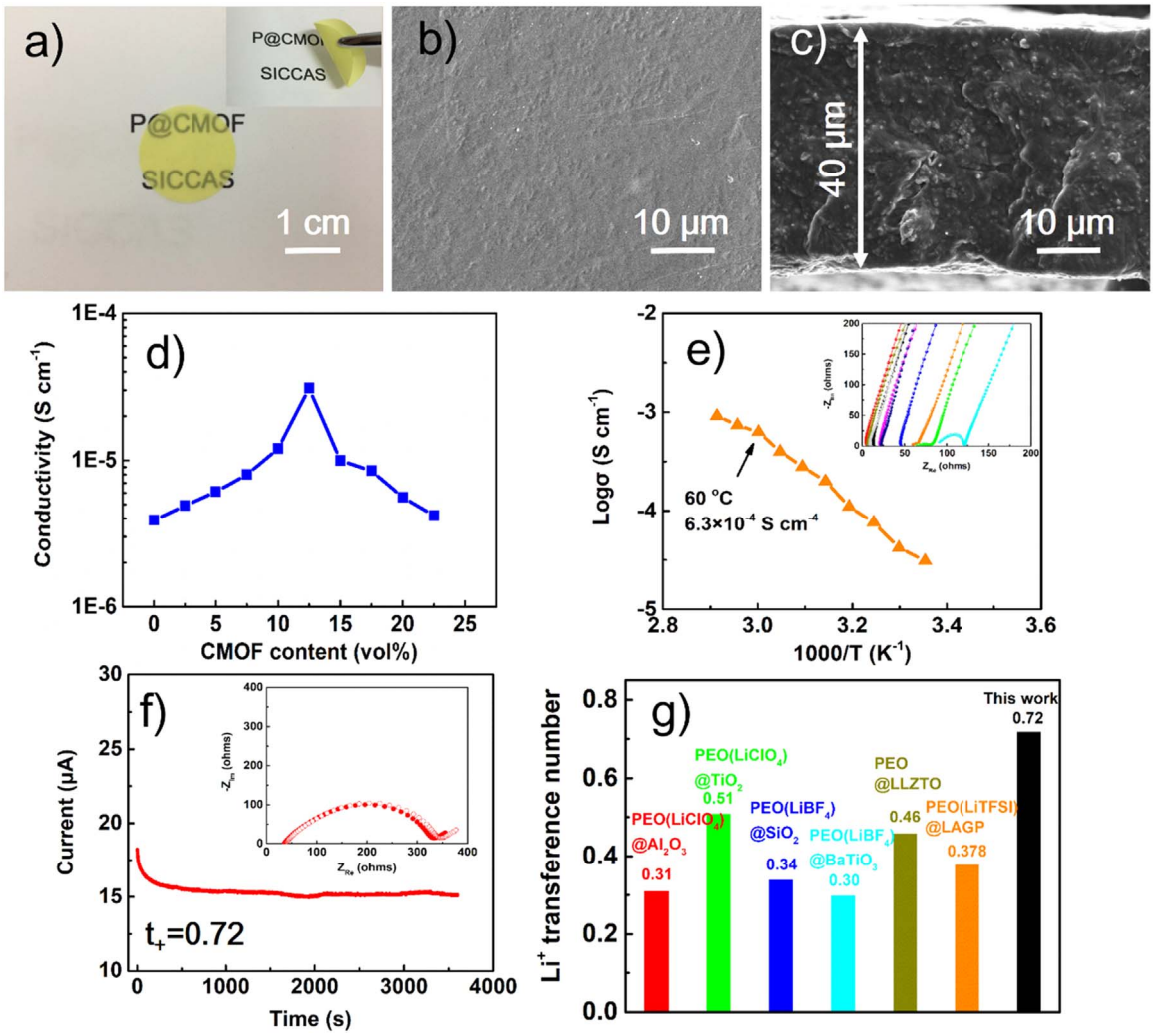

Fig. 2. a) Digital images of P@CMOF at flat and bended states (inset). b) Cross sectional and c) plane-view SEM images of P@CMOF. d) Ionic conductivities of P@CMOF with different content of COMF at room temperature (25 °C). e) Temperature dependent ionic conductivities of P@CMOF with 12.5 vol% CMOF. Inset: EIS of P@CMOF at temperature from 25 °C to 70 °C. f) t_+ of P@CMOF. g) t_+ of PEO($LiClO_4$)@Al_2O_3, PEO($LiClO_4$)@TiO_2, PEO($LiBF_4$)@SiO_2, PEO($LiBF_4$)@$BaTiO_3$, PEO@LLZTO, PEO(LiTFSI)@LATP, and P@CMOF (this work).

CMOF (Fig. S5) [38]. Fig. S6 displays the thermogravimetric analysis (TGA) of P@CMOF, showing a degradation temperature of 347 °C. The high thermal stability of P@CMOF is in sharp contrast to the organic liquid electrolytes with thermal instability and volatility. The tensile strength of P@CMOF with different contents of CMOF was investigated in Fig. S7. The tensile strength of pure PEO(LiTFSI) without CMOF is 2.5 MPa, which is consistent with the previous studies [39]. With the increasing content of CMOF from 0 to 20 vol%, the tensile strength of composite electrolytes increases from 2.5 to 9.7 MPa. The P@CMOF with improved mechanical strength is expected to exhibit enhanced dendrite suppression.

The ionic conductivity of composite electrolytes is a critical factor for their practical application in SSBs. In order to achieve high conductivity, the content of CMOF in P@CMOF was optimized. As shown in Fig. 2**d**, the conductivity of PEO(LiTFSI) without CMOF particles is 3.9×10^{-6} S cm^{-1} at 25 °C. With addition of CMOF, the conductivity of P@CMOF gradually increases due to the decreased PEO crystallinity. The melting temperature (T_m) of P@CMOF decreases from 62.1 °C to 56.3 °C with the increased content of CMOF from 0 vol% to 10 vol%, indicating more amorphous phase in the system (Fig. S8). Therefore, the movement of polymer chain segments and the migration of Li^+ are enhanced, leading to the improvement of conductivity [40]. When increasing the content of CMOF to 12.5 vol %, the conductivity reaches an optimal value of 3.1×10^{-5} S cm^{-1}. The Li^+ can not only migrate in the PEO matrix, but also an alternative highly conductive pathway along the interface between PEO and CMOF is available [41]. In addition, the fixed anion due to addition of CMOF can split the lithium salt ion pairs, increasing the Li^+ concentration and enhancing the conductivity of the electrolyte membranes. As Raman spectroscopy shown in Fig. S9, the dissociation degree of Li salt in P@CMOF with 12.5 vol% CMOF is 87.4%, which is higher than that of pure PEO(LiTFSI) [42]. Then, further adding CMOF results in the agglomeration of CMOF particles and the obstruction of interfacial pathway, thus sharply lowing the ionic conductivity. The conductivities with the temperature evolution from 25 °C to 70 °C were also investigated (Fig. 2**e** and Fig. S10). It shows some inflection plots and the slop of low temperature region (25–60 °C) and high temperature region (60–70 °C) are different. The different slops at low and high region could be attributed to the recrystallization of PEO polymer from the amorphous state when it's cooled down to the melting transition temperature of approximately 55 °C (Fig. S5). The ionic conductivity changes more obviously below the melting transition temperature due to the obviously changed crystallinity. While the whole polymer chain is almost amorphous at high temperature region (60–70 °C). The conductivity of P@CMOF approaches 6.3×10^{-4} S cm^{-1} at 60 °C, which is sufficient for application of SSBs. And it fits well with an Arrhenius plot in Fig. S11. The P@CMOF also shows low electrical conductivity according to potentiostatic polarization, which is 5 orders of magnitude

lower than the ionic conductivity (Fig. S12). In view of the results given above, the P@CMOF used as SPEs refers to P@CMOF with 12.5 vol% CMOF unless otherwise stated.

As shown in Fig. 2**f**, the P@CMOF possesses the Li^+ transference number (t_+) as high as 0.72, rendering sufficient fixed anion caused by electrostatic interaction of charge carriers. While the t_+ of PEO(LiTFSI) is 0.28, where the anion tends to free migration (Table S1). In addition, the t_+ is usually below 0.5 for the composite electrolytes comprising routine inorganic fillers (Fig. 2**g**) [6,43–45]. Doping highly-conductive electrolyte powders in PEO martrix, such as $Li_{6.4}La_3Zr_{1.4}Ta_{0.6}O_{12}$ (LLZTO) or $Li_{1.5}Al_{0.5}Ge_{1.5}(PO_4)_3$ (LAGP), is expected to obtain high t_+. It can not only conduct the Li^+ along the interface and polymer chain but provide the Li^+ pathway through the bulk phase. However, the t_+ are also as limited as 0.47 and 0.378, respectively (Fig. 2**g**) [46,47]. The low t_+ weakens the transport capability of cations due to the barrier of mobile anions, which leads to the dendritic Li deposition and propagation. In contrast, the high t_+ of P@CMOF is able to inhibit the formation of space charge near the Li anodes and guide Li^+ uniformly distribution [48].

To examine the long-term electrochemical stability of anion-immobilized P@CMOF against Li metal, the Li symmetrical cells were assembled. Prior to the test, The interfacial compatibility between electrolytes and Li metal anodes was tested [14]. As the EIS of Li/P@CMOF/Li cells shown in Fig. S13 (Supporting information), the resistance value of cells has no obvious change before and after 10 days at 60 °C, indicating the chemical stability of P@CMOF towards Li metal. The symmetrical cells were cycled at a current density of 0.1 mA cm^{-2} at 60 °C. In Fig. 3**a**, the cells exhibit an excellent cycle stability for 400 h with a nearly constant polarization voltage of 0.07 V. The interfacial resistance of the passivation film Rf, and charge-transfer resistance Rct before cycling are 44.5 Ω cm^2 and 42.4 Ω cm^2, respectively (Fig. S14 and Table S2). The resistances decreases to 41.4 Ω cm^2 and 40.4 Ω cm^2 after initial several cycles, mainly owing to the interfacial activation [49]. The values slightly increase to 44.2 Ω cm^2 and 45.8 Ω cm^2 after 400 h, suggesting a stable interface. This could be ascribed to the uniform Li plating and striping, originating from anion-immobilized effect of P@CMOF. Without the disturbance from free anions, the Li^+ can fast diffuse evenly in the electrolyte membrane and then deposit on the surface of Li metal uniformly. According to the simulation of Finite element method (FEM), P@CMOF shows small concentration gradients of both Li^+ and anions during Li deposition (Figs. 4**a** and 4**b**). The homogenous environment from the bulk membrane to the surface of Li metal avoid the formation of large electric field, and hence induces the dendrite-free Li deposition (Fig. 4**c**) [15,50]. In addition, the large-surface-area CMOF particles doped in PEO polymer provide an intimate contact between electrolyte and Li metal, and serve as mechanical barriers to block the propagation of Li dendrites [51]. The effect of P@CMOF for dendrite-free Li deposition is evidenced by SEM image in Fig. 3**d**. A flat surface of Li metal is observed after 400 h, indicating uniform Li plating and stripping process.

In contrast, the polarization voltage of Li symmetrical cells with PEO(LiTFSI) is 0.28 V in the first cycle and sharply decreases to near 0 V after 77 h cycling at 0.1 mA cm^{-2} (Figs. 3**b** and 3**c**). The short circuit

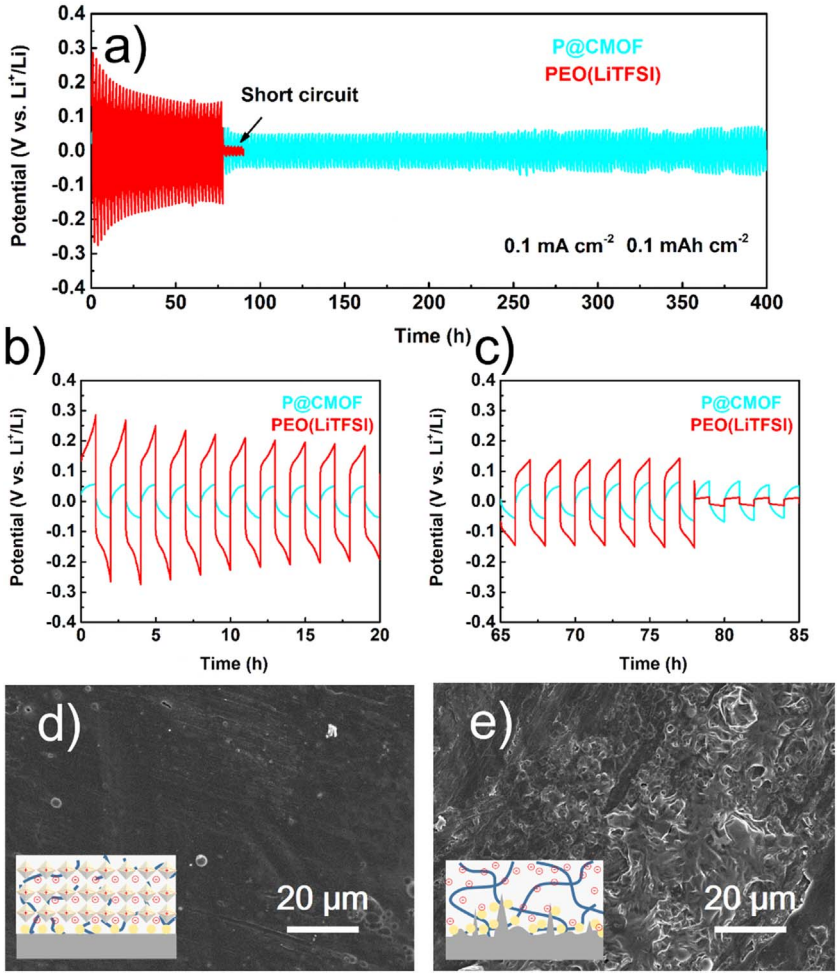

Fig. 3. a) Galvanostatic cycles with a constant current density of 0.1 mA cm^{-2} for Li/P@CMOF/Li and Li/PEO(LiTFSI)/Li cells at 60 °C. Magnification of Galvanostatic cycles from b) 0 h to 20 h and c) 65 h to 85 h. d) Plane view SEM of Li anode for Li/P@CMOF/Li cell after 400 h cycles. e) Plane view SEM of Li anode for Li/PEO(LiTFSI)/Li cell after short circuiting.

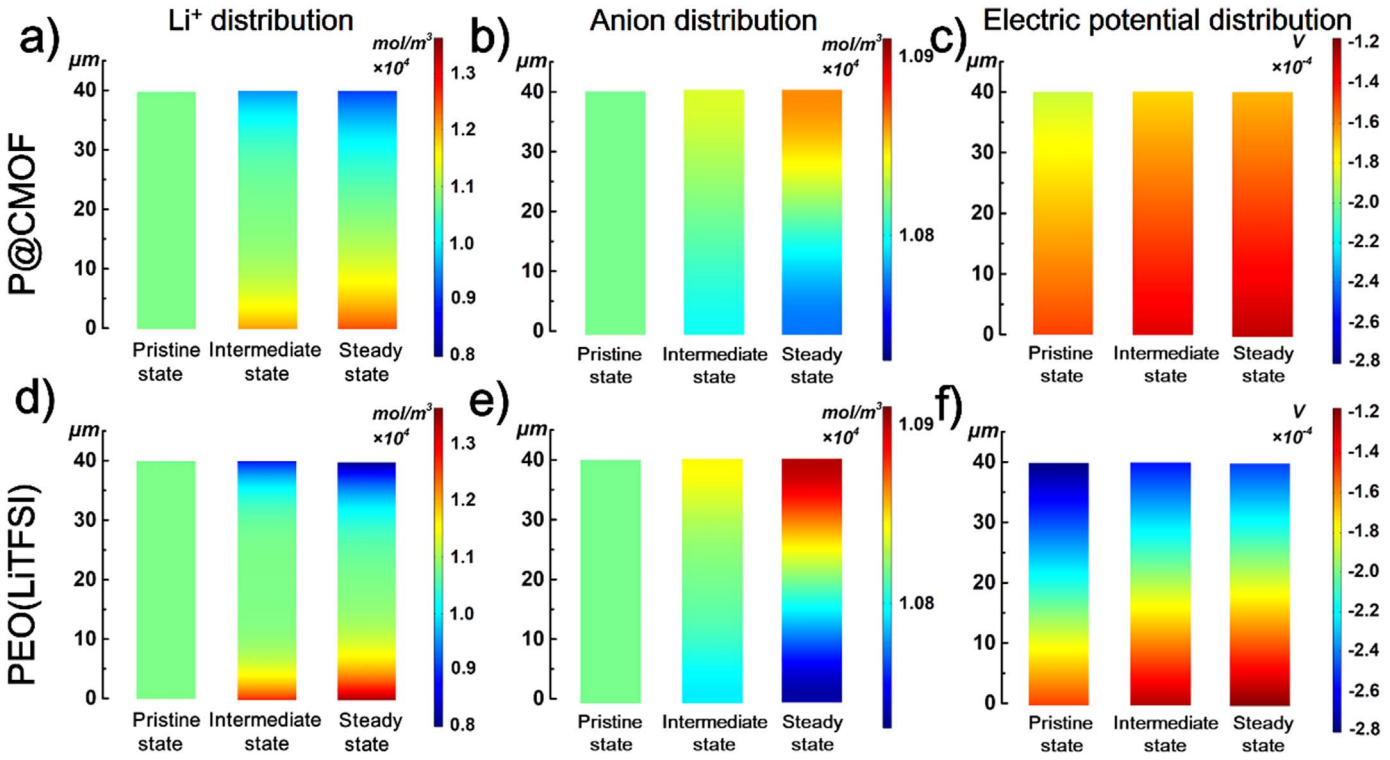

Fig. 4. Distribution of Li^+, anion and electric potential in a-c) P@CMOF and d-e) PEO(LiTFSI) at pristine state, intermediate state, and steady state during Li deposition at 0.1 mA cm^{-2}. These results were obtained by Finite element method (FEM).

of working batteries is blamed for the low t_+ of PEO(LiTFSI), which possesses plenty of free anions. The anions tend to hinder the Li^+ fast migration due to their opposite moving direction, leaving a much larger Li^+ concentration gradient than that of P@CMOF (Fig. 4**d**). Furthermore, the anion depletion near Li metal anodes induces the development of space charge, which produces a large electric field (Figs. 4**e** and 4**f**). The as-obtained electric field results in the uneven Li deposition and dendrite growth [15,48]. Therefore, the Li dendrites propagate and new preferential deposition spots appear, which leads to short circuit of the SSBs as a consequence. As shown in Fig. 3**e**, mossy-like Li dendrites are clearly observed on the surface of Li metal anode after short circuit. When the current density increasing to 0.5 mA cm^{-2}, the Li symmetrical cells with anion-immobilized P@CMOF can be continuously operated for 200 h with the polarization voltage of 0.12 V (Fig. S15a and S15c). It can be attributed to the homogenous Li deposition and sustainable electrolyte/Li anode interface. The cells with PEO(LiTFSI) show the polarization of 0.31 V at 0.5 mA cm^{-2} for the first cycle. The polarization becomes too severe to operate the battery for the next cycles (Fig. S15a and S15b). Such poor performance compared with the cells with P@CMOF results from hindered transport of Li^+ and uneven Li deposition.

The feasibility of the P@CMOF in SSBs was examined by Li metal coupled with $LiFePO_4$ (LFP) cathodes as example. Fig. 5**a** shows the flat potential plateaus with the polarization of 0.06 V when charging and discharging at 0.1 C and 60 °C, which is lower than that of cells with PEO (LiTFSI). The initial coulomic efficiency of cells with P@CMOF is 93.7%, higher than 90.1% of cells with PEO(LiTFSI). In addition, the specific discharge capacity for cells with P@CMOF is 141.2 mAh g^{-1} at 0.1 C. The cells with P@CMOF deliver the discharge capacities of 126.4 mAh g^{-1}, 106.3 mAh g^{-1}, 88.0 mAh g^{-1}, 67.4 mAh g^{-1}, at 0.5 C, 1 C, 2 C, 5 C, respectively (Fig. 5**b**). This excellent performance outperforms previous designs (Table S3). Due to the anion immobilization of P@CMOF, the flat surfaces of Li metal anodes without obvious dendrites are observed after 10 cycles at various rates (Fig. S16). After the end of high rate cycling at 5 C, the discharge capacity could still be recovered to 107.1 mAh g^{-1} as the current density turns back to 1 C. In contrast, the cells with PEO(LiTFSI) deliver the discharge capacities of 135.1 mAh g^{-1}, and 100.8 mAh g^{-1} at 0.1 C and 0.5 C, respectively. The discharge capacity suddenly decreases from 63.2 mAh g^{-1} to 17.6 mAh g^{-1} after several cycles at 1 C. The low capacity and poor cycling stability could be attributed to hindered migration of Li^+, uneven Li deposition, and poor interfacial property. With the anion-immobilized P@CMOF and dendrite-free Li anode, the SSBs with LFP cathodes can be charged and discharged for 300 cycles with a capacity retention of 85.4% at 1 C (Fig. 5**c**).

High-voltage SSBs have received great attention for providing improved energy density. Wide electrochemical window of solid electrolytes is a prerequisite, which can be examined by linear sweep voltammetry (LSV). As shown in Fig. 5**d**, the oxidation process commences at 4.13 V for the PEO(LiTFSI). This could be attributed to the ether oxygen in PEO chains, which is easy to be oxidized at high voltage [52]. The P@CMOF exhibits an electrochemical window as high as 4.97 V. The key lies in the hydrogen bonds between ether oxygen of PEO chains and -NH_2 group of CMOF, leading to a protected ether oxygen and stable composite structure at high voltage (Fig. S17a) [23]. In addition, the use of large-specific-area CMOF particles also helps to remove the impurities at interfaces [53]. To confirm the effect of hydrogen bonds in widening electrochemical window, The UiO-66, D-UiO-66-NH_2, CMOF without -NH_2 group were also dispersed in PEO polymers to fabricate composite electrolyte (Fig. S17b). The electrochemical windows of UiO-66 and CMOF without -NH_2 group show no obvious improvement in comparison with those of D-UiO-66-NH_2 and CMOF grafted -NH_2 group in Fig. 5**d** and Fig. S18. We assembled the pouch cell with high-voltage $LiFe_{0.15}Mn_{0.85}PO_4$ (LFMP) cathodes and P@CMOF, which was charged to 4.4 V (Fig. S19a). The initial coulomic efficiency is 94.1% at 0.1 C, and a capacity retention of 81.2% is achieved after 100 cycles (Fig. 5**e** and Fig. S19b). In addition, the light emitting diode (LED) with the signal of "SICCAS" can be successfully lighted whenever the pouch cell is at flatting or bending state, rendering the ability of P@CMOF to be applied in flexible electronics

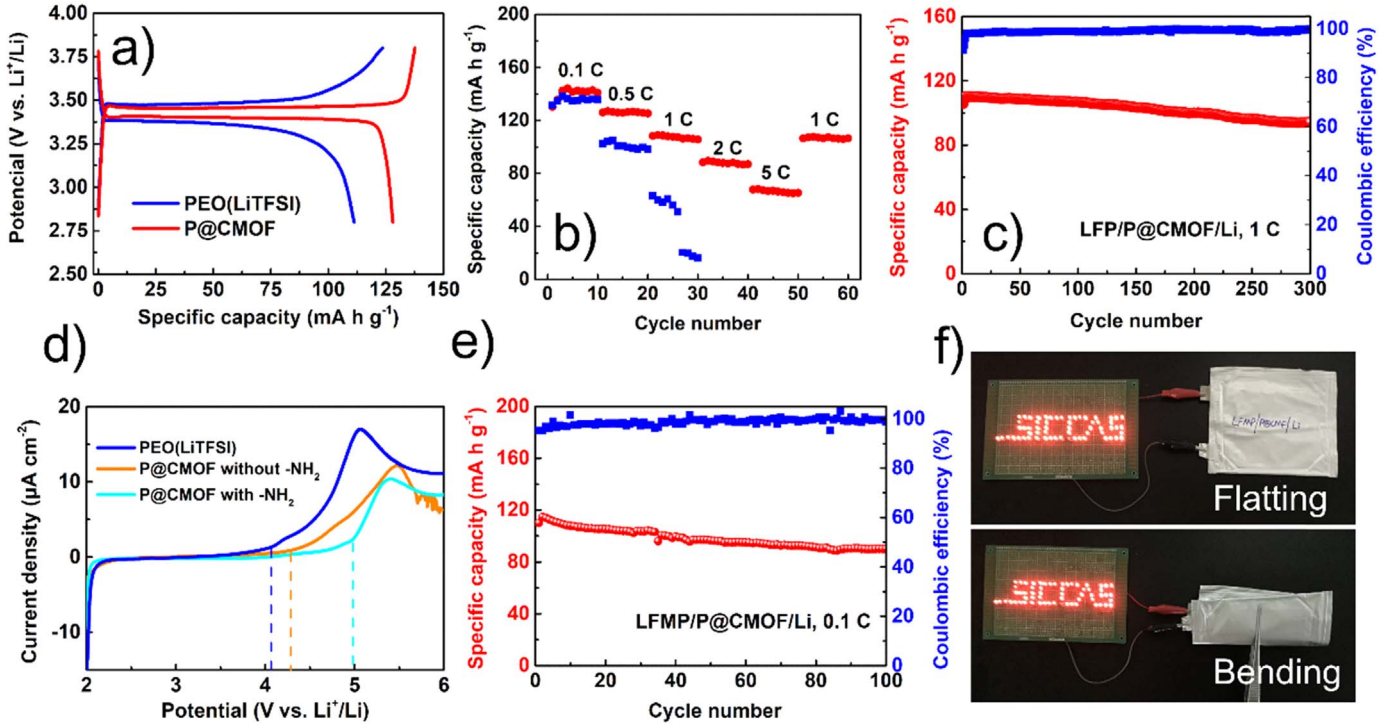

Fig. 5. a) Charge-discharge curves of first cycle at 0.1 C for LFP/P@CMOF/Li and LFP/PEO(LiTFSI)/Li cells at 60 °C. b) Specific capacities at various rates for LFP/P@CMOF/Li and LFP/PEO(LiiTFSI)/Li cells. c) Cycle performance at 1 C for LFP/P@CMOF/Li cell at 60 °C. d) LSV scans for PEO(LiTFSI), P@CMOF with -NH_2 and P@CMOF without -NH_2. e) Cycle performance at 0.1 C for LFMP/P@CMOF/Li pouch cell at 60 °C. f) Illustration of the pouch cell for powering the LEDs with the signal of "SICCAS" at flatting and bending state.

(Fig. 5**f**). Therefore, the P@CMOF can not only suppress Li dendrites in SSBs, but also shows the potential in flexible devices with enhanced energy density.

4. Conclusions

In summary, we proposed a novel cationic metal-organic framework in polymer electrolyte to immobilize anions via electrostatic interaction and inhibit lithium dendrites in solid-state batteries. The P@CMOF shows a remarkable improvements in ionic conductivity at both room and elevated temperature due to the addition of CMOF. It exhibits a high t_+ of 0.72 and wide electrochemical window of 4.97 V. According to the simulation of finite element method, small concentration gradients of both Li^+ and anions are obtained in the anion-immobilized electrolyte, which prevents the formation of a large electrical field caused by space charge. Therefore, a uniform Li plating/stripping without discernable dendrites is obtained at 0.1 mA cm^{-2} and 0.5 mA cm^{-2}. The SSBs with $LiFePO_4$ cathodes render a high capacity retention of 85.4% after 300 cycles at 1 C. Furthermore, the wide electrochemical window of P@CMOF enables the usage of high-voltage $LiFe_{0.15}Mn_{0.85}PO_4$ cathodes. Anion immobilization via electrostatic interaction opens a new avenue to understand the growth and suppression of Li dendrites in SSBs. In addition, design of novel cationic fillers for anion immobilization can be easily scalable to other MOF structures, which are expected to achieve the same or even better electrochemical performances.

Acknowledgements

The authors would like to thank the National Natural Science Foundation of China (Grant No. 51771222, 51532002 and 21606215), the National Key R & D Program of China (Grant No. 2018YFB0104300), the Synchrotron-Radiation Joint Funds of University of Science & Technology of China (No. NSRLLHJJ2016) and the "Taishan Scholars Program".

Appendix A. Supplementary material

Supplementary data associated with this article can be found in the online version at doi:10.1016/j.ensm.2019.01.007

References

[1] J.-M. Tarascon, M. Armand, Nature 414 (2001) 359–367.
[2] P.V. Wright, Polym. Int. 7 (1975) 319–327.
[3] C.W. Liew, R. Durairaj, S. Ramesh, PLoS One 9 (2014) e102815.
[4] W.H. Meyer, Adv. Mater. 10 (1998) 439–448.
[5] K. Vignarooban, M. Dissanayake, I. Albinsson, B.-E. Mellander, Solid State Ion. 266 (2014) 25–28.
[6] C.W. Lin, C.L. Hung, M. Venkateswarlu, B.J. Hwang, J. Power Sources 146 (2005) 397–401.
[7] D. Lin, W. Liu, Y. Liu, H.R. Lee, P.C. Hsu, K. Liu, Y. Cui, Nano Lett. 16 (2016) 459–465.
[8] J. Chai, B. Chen, F. Xian, P. Wang, H. Du, J. Zhang, Z. Liu, H. Zhang, S. Dong, X. Zhou, Small 14 (2018) 1802244.
[9] X.B. Cheng, R. Zhang, C.Z. Zhao, Q. Zhang, Chem. Rev. 117 (2017) 10403–10473.
[10] Z. Hu, S. Zhang, S. Dong, W. Li, H. Li, G. Cui, L. Chen, Chem. Mater. 29 (2017) 4682–4689.
[11] S.-S. Chi, Y. Liu, N. Zhao, X. Guo, C.-W. Nan, L.-Z. Fan, Energy Storage Mater. (2018).
[12] L. Chen, Y. Liu, L.-Z. Fan, J. Electrochem. Soc. 164 (2017) A1834–A1840.
[13] C. Monroe, J. Newman, J. Electrochem. Soc. 152 (2005) A396.
[14] X. Han, Y. Gong, K.K. Fu, X. He, G.T. Hitz, J. Dai, A. Pearse, B. Liu, H. Wang, G. Rubloff, Y. Mo, V. Thangadurai, E.D. Wachsman, L. Hu, Nat. Mater. 16 (2017) 572–579.
[15] Z. Tu, P. Nath, Y. Lu, M.D. Tikekar, L.A. Archer, Acc. Chem. Res. 48 (2015) 2947–2956.
[16] C. Brissot, M. Rosso, J.-N. Chazalviel, S. Lascaud, J. Power Sources 81 (1999) 925–929.
[17] L. Yue, J. Ma, J. Zhang, J. Zhao, S. Dong, Z. Liu, G. Cui, L. Chen, Energy Storage Mater. 5 (2016) 139–164.
[18] F. Croce, L. Settimi, B. Scrosati, Electrochem. Commun. 8 (2006) 364–368.
[19] F. Croce, L. Persi, B. Scrosati, F. Serraino-Fiory, E. Plichta, M. Hendrickson, Electrochim. Acta 46 (2001) 2457–2461.
[20] C. Yuan, J. Li, P. Han, Y. Lai, Z. Zhang, J. Liu, J. Power Sources 240 (2013) 653–658.
[21] M.J. Katz, Z.J. Brown, Y.J. Colón, P.W. Siu, K.A. Scheidt, R.Q. Snurr, J.T. Hupp, O.K. Farha, Chem. Commun. 49 (2013) 9449.
[22] J.H. Cavka, S. Jakobsen, U. Olsbye, N. Guillou, C. Lamberti, S. Bordiga, K.P. Lillerud, J. Am. Chem. Soc. 130 (2008) 13850–13851.

[23] J. Tanthana, S.S. Chuang, ChemSusChem 3 (2010) 957–964.
[24] J.F. Bunnett, R.E. Zahler, Chem. Rev. 49 (1951) 273–412.
[25] A. Matsumoto, K. Sada, K. Tashiro, M. Miyata, T. Tsubouchi, T. Tanaka, T. Odani, S. Nagahama, T. Tanaka, K. Inoue, Angew. Chem. Int. Ed. 41 (2002) 2502–2505.
[26] M. Badila, C. Brochon, A. Hebraud, G. Hadziioannou, Polymer 49 (2008) 4529–4533.
[27] M. Shukur, F. Ibrahim, N. Majid, R. Ithnin, M. Kadir, Phys. Scr. 88 (2013) 025601.
[28] L. Valenzano, B. Civalleri, S. Chavan, S. Bordiga, M.H. Nilsen, S. Jakobsen, K.P. Lillerud, C. Lamberti, Chem. Mater. 23 (2011) 1700–1718.
[29] Z. Wang, S.M. Cohen, Angew. Chem. 120 (2008) 4777–4780.
[30] Y. Ma, R. Matsuda, H. Sato, Y. Hijikata, L. Li, S. Kusaka, M. Foo, F. Xue, G. Akiyama, R. Yuan, J. Am. Chem. Soc. 137 (2015) 15825–15832.
[31] G.W. Peterson, J.J. Mahle, J.B. DeCoste, W.O. Gordon, J.A. Rossin, Angew. Chem. Int. Ed. 55 (2016) 6235–6238.
[32] T. Steiner, Angew. Chem. Int. Ed. 41 (2002) 48–76.
[33] X. Wang, W. Chen, L. Zhang, T. Yao, W. Liu, Y. Lin, H. Ju, J. Dong, L. Zheng, W. Yan, J. Am. Chem. Soc. 139 (2017) 9419–9422.
[34] H. Huo, N. Zhao, J. Sun, F. Du, Y. Li, X. Guo, J. Power Sources 372 (2017) 1–7.
[35] P. Zhang, L.C. Yang, L.L. Li, M.L. Ding, Y.P. Wu, R. Holze, J. Membr. Sci. 379 (2011) 80–85.
[36] H. Yamada, A.J. Bhattacharyya, J. Maier, Adv. Funct. Mater. 16 (2006) 525–530.
[37] Y. Yamada, K. Furukawa, K. Sodeyama, K. Kikuchi, M. Yaegashi, Y. Tateyama, A. Yamada, J. Am. Chem. Soc. 136 (2014) 5039–5046.
[38] K.W. Chapman, G.J. Halder, P.J. Chupas, J. Am. Chem. Soc. 130 (2008) 10524–10526.
[39] J. Zhang, J. Zhao, L. Yue, Q. Wang, J. Chai, Z. Liu, X. Zhou, H. Li, Y. Guo, G. Cui, L. Chen, Adv. Energy Mater. 5 (2015) 1501082.
[40] J.H. Ahn, G.X. Wang, H.K. Liu, S.X. Dou, J. Power Sources 119-121 (2003) 422–426.
[41] L. Chen, Y. Li, S.-P. Li, L.-Z. Fan, C.-W. Nan, J.B. Goodenough, Nano Energy 46 (2018) 176–184.
[42] H. Huo, J. Sun, C. chen, X. Meng, M. He, N. Zhao, X. Guo, J. Power Sources 383 (2018) 150–156.
[43] F. Croce, L. Persi, F. Ronci, B. Scrosati, Solid State Ion. 135 (2000) 47–52.
[44] Y. Liu, J.Y. Lee, L. Hong, J. Power Sources 129 (2004) 303–311.
[45] H. Sun, Y. Takeda, N. Imanishi, O. Yamamoto, H.J. Sohn, J. Electrochem. Soc. 147 (2000) 2462–2467.
[46] S. Chen, Y. Zhao, J. Yang, L. Yao, X. Xu, Ionics 23 (2016) 2603–2611.
[47] J. Zhang, N. Zhao, M. Zhang, Y. Li, P.K. Chu, X. Guo, Z. Di, X. Wang, H. Li, Nano Energy 28 (2016) 447–454.
[48] C.Z. Zhao, X.Q. Zhang, X.B. Cheng, R. Zhang, R. Xu, P.Y. Chen, H.J. Peng, J.Q. Huang, Q. Zhang, Proc. Natl. Acad. Sci. USA 114 (2017) 11069–11074.
[49] L. Wang, L. Zhang, Q. Wang, W. Li, B. Wu, W. Jia, Y. Wang, J. Li, H. Li, Energy Storage Mater. (2017).
[50] J.N. Chazalviel, Phys. Rev. A 42 (1990) 7355–7367.
[51] C. Wang, H. Xie, L. Zhang, Y. Gong, G. Pastel, J. Dai, B. Liu, E.D. Wachsman, L. Hu, Adv. Energy Mater. (2017) 1701963.
[52] Z. Xue, D. He, X. Xie, J. Mater. Chem. A 3 (2015) 19218–19253.
[53] A. Manuel Stephan, K.S. Nahm, Polymer 47 (2006) 5952–5964.